J Therm Anal Calorim (2011) 106:463–467
DOI 10.1007/s10973-011-1503-z

Correlations between data of ^{29}Si NMR and thermogravimetry for silica/monetite nanocomposites

A. J. D. Fernandes · J. H. P. Barbosa · O. G. Silva · M. G. Fonseca · L. H. N. Arakaki · J. G. P. Espínola

CBRATEC7 Conference Special Issue

Abstract Silica/monetite nanocomposites were synthesized through controlled hydrolysis of tetraethoxysilane at concentrations of 5, 10, 15, and 20% mol/mol of calcium phosphate forming the solids named CaPSil1, CaPSil2, CaPSil3, and CaPSil4, respectively. XRD patterns showed formation of nanocomposites with a decrease in crystallinity. The NMR ^{29}Si spectra suggested an increase in the content of incorporated silica with reduction of Q^3 (–SiOH) signal, which contributes for mass loss, in agreement with thermogravimetry. The incorporation of silica increased the chemical stability of the precursor phosphate in an acidic medium.

Keywords Silica/monetite nanocomposites · Thermogravimetry · Calcium phosphate

Introduction

The surface modification of calcium phosphates using alkoxide silane precursors allows formation of solids with pure composition SiO_2–CaO–P_2O_5. The new compounds improve their physicochemical properties showing better colloidal stability, resistance to dissolution in acid media, and bioactivity, which can foment a bone formation in the interface of the material [1]. This bioactivity is due to the high density of silanol groups (Si–OH) on the surface of silica, those being good nucleation sites for hydroxyapatite (HAP) ($Ca_{10}(PO_4)_6(OH)_2$) [2]. Therefore, these materials show enhanced characteristics and can be used as biomaterials for bone substitution in implants and grafts [3].

In this study, silica/monetite nanocomposites were obtained through the sol–gel method, using the controlled hydrolysis of tetraethoxysilane (TEOS) at concentrations of 5, 10, 15, and 20% mol/mol of calcium phosphate, whose structural and morphological characterization was done by X-ray diffractometry (XRD), infrared (IR) spectroscopy, thermogravimetry (TG) and nuclear magnetic resonance (^{29}Si NMR). The chemical stability was implemented for pH varying at 1.0–6.0.

Methods and materials

Chemicals

Reagents with analytic grade were applied in all procedures. Dihydrated calcium chloride $CaCl_2{\cdot}2H_2O$ (VETEC, P.A.), dibasic ammonium phosphate $(NH_4)_2HPO_4$ (REAGEN, P.A.), and TEOS, $Si(OCH_2CH_3)_4$ (MERCK, P.A) were used as received without previous purification.

37% Hydrochloric acid (HCl), potassium chloride (KCl), potassium biphtalate ($C_8H_5O_4K$), and sodium hydroxide (NaOH) (all from Merck) were employed in the buffer solution preparations for chemical stability tests. Deionized water and ethanol (Merck) were used as solvents.

Synthesis of monetite and nanocomposites

Monetite ($CaHPO_4$) was synthesized as a control by precipitation method by mixing two aqueous solutions of $(NH_4)_2HPO_4$ and $CaCl_2$ with Ca/P at 1:1 ratio. First, 100.0 cm^3 of $(NH_4)_2HPO_4$ 0.050 mol dm^{-3} was heated at

A. J. D. Fernandes (✉) · J. H. P. Barbosa · O. G. Silva · M. G. Fonseca · L. H. N. Arakaki · J. G. P. Espínola
Department of Chemistry, CCEN, UFPB, João Pessoa, Brazil
e-mail: anejfernandes@yahoo.com.br

373 ± 10 K under reflux and stirring. To this hot solution, 25.0 dm^3 of $CaCl_2$ 0.10 mol dm^{-3} was slowly added and immediately a white suspension was formed and the suspension was aged for 24 h at 373 K. The white solid was separated by filtration, washed successively with water until a detection of negative chlorite test in the filtrated portion using silver nitrate solution. Finally, the solid named CaP was dried at 573 ± 10 K during 24 h.

The synthesis of nanocomposites followed the same method using TEOS dissolved in ethanol at concentrations of 5, 10, 15, and 20% in mol of monetite. The solids were dried at 320 ± 10 K for 24 h, being identified as CaPSil1, CaPSil2, CaPSil3, and CaPSil4 for solids prepared with 5, 10, 15, and 20% of TEOS, respectively.

The solids were characterized by XRD, IR spectroscopy, thermogravimetry, and ^{29}Si NMR.

Physical measurements

XRD patterns were obtained with nickel-filtered CuKα radiation on a Shimadzu diffractometer model XD3A operating at 40 kV and 30 mA with a scan rate of 0.67° s^{-1} in the range $2\theta = 1.5$–70°. IR spectra were obtained on a Bomem spectrometer, MB series, using KBr-pressed samples, between 4000 and 400 cm^{-1} with a 4 cm^{-1} resolution and 30 scans for each run. Thermal analyses were performed on a thermogravimetry DuPont apparatus, model 1090 B, coupled with a thermobalance 951 heated to 1273 K, programmed with a heating rate of 0.17 K s^{-1} in a dry-nitrogen atmosphere. The samples varied in weight from 15.0 to 30.0 mg. Si^{29} NMR spectra were obtained with an AC 300/P Bruker spectrophotometer, using the HPDEC (high-power decoupling) technique at 79.49 MHz, acquisition time of 5 s, contact time of 4 ms and 90° of pulse width.

Stability tests

The stability of solids was tested by suspending a series of 100.0 mg samples of each solid in 25.0 cm^3 of a buffer solution. The series of buffer solutions with well-established pH values of 1.00, 3.03, 4.03, 5.00, and 6.09 were used. The suspensions were mechanically stirred for 48 h at 298 ± 1 K and each solid was separated by centrifugation and dried at 393 K. The content of calcium was determined in duplicate for each sample of the supernatant using an absorption atomic instrument of GBC 808 AA model.

Results

This study is focused on functionalized calcium phosphate ($CaHPO_4$) with silica and their new properties; the characterization of which was performed through XRD, thermogravimetry, infrared spectroscopy, and ^{29}Si NMR.

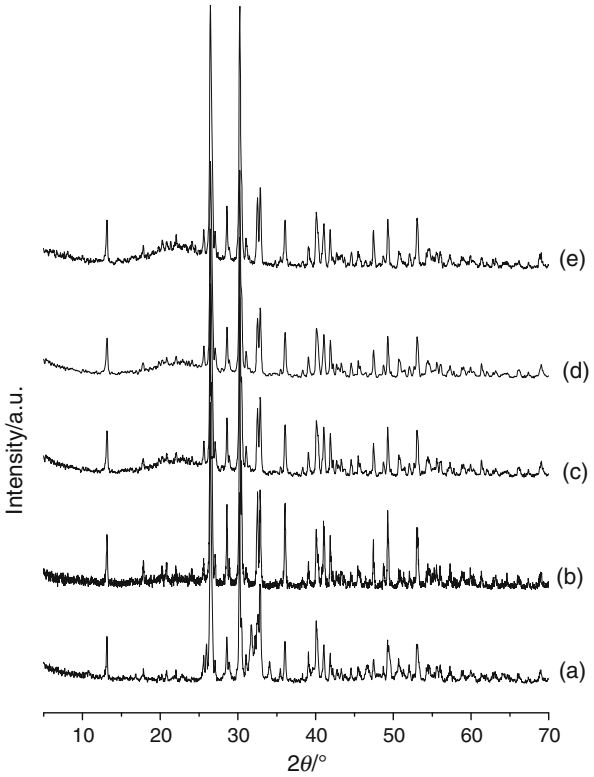

Fig. 1 XRD for (*a*) monetite, (*b*) CaPSil1, (*c*) CaPSil2, (*d*) CaPSil3, and (*e*) CaPSil4

The diffractograms of pure calcium phosphate or monetite ($CaHPO_4$) (Fig. 1) confirm the formation of a single phase (JCPDS 01-070-0359). The entrance of silica onto phosphate structure through the TEOS hydrolysis generated a reduction in the crystallinity of the final solids. Small variations in the interlamelar spacing in pure monetite (0.6737 nm) compared with other solids (0.6731 nm) were detected suggesting that the silica was anchored onto phosphate surface.

The IR spectrum (Fig. 2) showed that for the precursor phosphate the main absorption bands and their attributions occur at 3700–3500 cm^{-1} due to the stretching vibration of O–H of water and structural OH; at 1620 cm^{-1} associated O–H bending of water; at 1087, 1030, 956 attributed to asymmetric stretching of PO_4^{3-} and 865 cm^{-1} associated to the stretching of P–O(H) in $H_2PO_4^-$ [4–6]. Another absorption in cm^{-1} occurred at 610 cm^{-1} corresponding to asymmetric stretching of P–O of the group PO_4^{3-} and the bands at 560 and 450 cm^{-1}, due to an asymmetric stretching of P–O(H) of the group HPO_4^{2-} [5, 6]. The IR spectra for nanocomposites showed all bands of monetite with the appearance of new bands at 1110 cm^{-1}, attributed to the stretching vibration of Si–O–Si (siloxane), and at

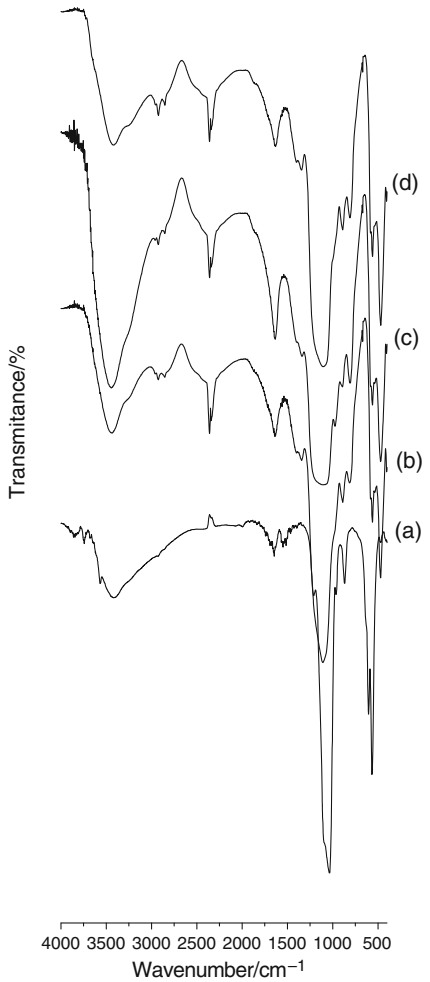

Fig. 2 FTIR spectra for (*a*) monetite, (*b*) CaPSil1, (*c*) CaPSil2, (*d*) CaPSil3, and (*e*) CaPSil4

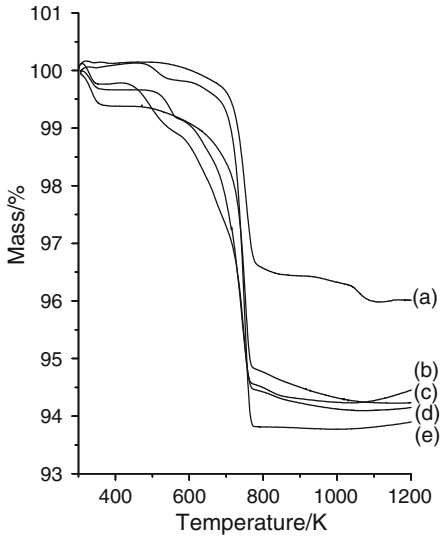

Fig. 3 Thermogravimetry of (*a*) monetite, (*b*) CaPSil4, (*c*) CaPSil3, (*d*) CaPSil2, and (*e*) CaPSil1

Table 1 Data of thermogravimetry for nanocomposites of monetite and silica

Solid	Temperature range/K	Mass loss/%
Monetite	300–350	0.10
	680–790	3.50
CaPSil1	300–361	0.34
	457–550	0.28
	640–781	5.49
CaPSil2	300–360	0.52
	473–564	0.52
	564–1009	4.82
CaPSil3	300–368	0.59
	450–1100	5.17
CaPSil4	300–348	0.22
	399–568	0.89
	568–695	1.57
	695–971	2.89

970 cm^{-1}, due to the deformation of free silanol groups Si–OH [7]. Other bands at 2950 and 2850 cm^{-1} were due to asymmetric and symmetric stretching, respectively of C–H [8]. The two last bands are the indication of non-hydrolyzed alkoxide groups which can be eliminated by calcinations of powders. These data are in agreement with covalent incorporation of silica onto phosphate surface through the condensation of $(_3HCCH_2O)_4Si$ and P–OH forming P–OSiOH or P–OSiOSiOH.

Thermogravimetry of pure monetite showed a total mass loss of 3.9% with two events of decomposition: (i) for 300–350 K, referred to evaporation of absorbed water and (ii) for 680–790 K due to the transformation of monetite to α-$Ca_2P_2O_7$, through the condensation of the group HPO_4^{2-}. The thermogravimetry curves for the modified phosphates, in Fig. 3, showed a degradation process in non-defined stages showing a total mass loss of 6.2, 5.9, 5.7, and 5.8%, respectively for CaPSil1, CaPSil2, CaPSil3, and CaPSil24. These data indicated that the total mass losses were independent of the content of incorporated silica suggesting that the entrance of silica was via OH^- groups of phosphate which condense between 640 and 780 K. The intervals of temperature for decompositions of composites showed no drastic differences. The first losses were attributed to the exit of absorbed water, the second to the condensation of the OH^- groups of phosphate, silica and non-condensing organic groups, and the third related to isolated OH^- groups. These data are summarized in Table 1.

According to the ^{29}Si NMR spectra (Fig. 4), all nanocomposites showed three peaks attributed to Q^4, Q^3, and Q^2

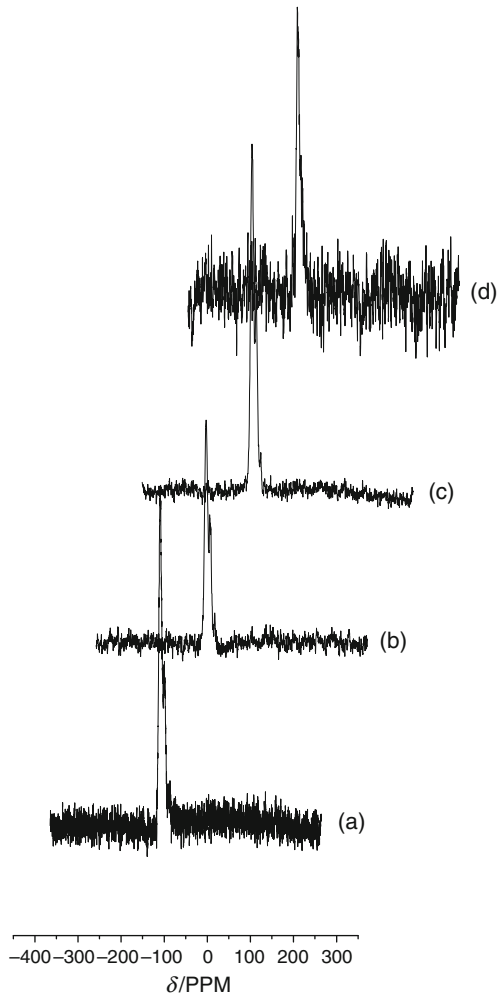

Fig. 4 NMR ^{29}Si spectra for (*a*) CaPSil1, (*b*) CaPSil2, (*c*) CaPSil3, and (*d*) CaPSil4

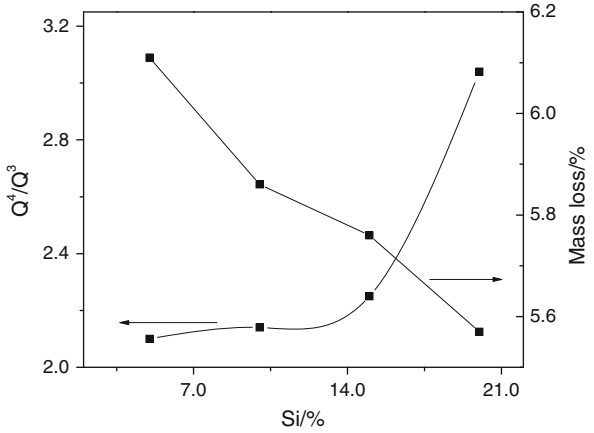

Fig. 5 Correlation between the content of silicon of nanocomposites, total mass loss data, and NMR ^{29}Si

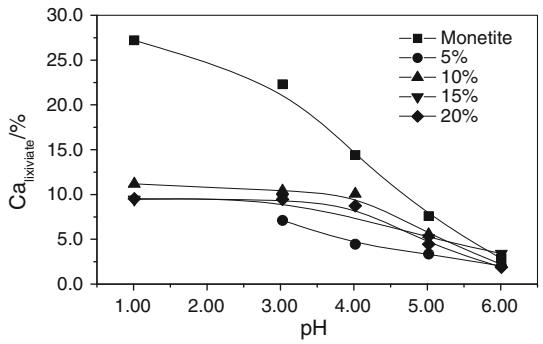

Fig. 6 Content of calcium for pure monetite and silica/calcium phosphates nanocomposites after exposited 48 h at controlled pH

species with the most abundant signal being associated to Q^4 siloxane and the lower one related to Q^2 species as summarized in Table 2.

Thermogravimetry indicated that CaPSil1 showed a high mass loss. Therefore, CaPSil1 showed the high content for Q^3 species relating to silanol groups. In this case, the condensation of silanol groups contributes substantially to the events of thermodecomposition of the material. Similarly, CaPSil4 had a low content of Q^3 species, which showed a low total mass loss (Fig. 5).

It suggests that a high content of incorporated silica was associated with an increase in the concentration of siloxane groups indicating a better polymerization of silica onto phosphate surface. Therefore, a high content of these species results in a low mass loss in thermogravimetry. This indicates that silica was covalently linked to phosphate contributing to improvement in the chemical stability of the solid compared with original

Table 2 Quantity of Q^4, Q^3, and Q^2 silicon species for nanocomposites estimated by deconvolution of the ^{29}Si NMR

Sample	Q^4		Q^3		Q^2		Q^4/Q^3
	Area	δ/ppm (Error/%)	Area	δ/ppm (Error/%)	Area	δ/ppm (Error/%)	
CaPSil1	3.66×10^9	−109.05 (0.03)	1.74×10^9	−99.70 (0.08)	1.78×10^8	−88.41 (0.15)	2.10
CaPSil2	2.53×10^9	−109.11 (0.03)	1.18×10^9	−100.09 (0.04)	9.84×10^7	−89.28 (0.02)	2.14
CaPSil3	2.68×10^9	−109.17 (0.01)	1.19×10^9	−99.75 (0.03)	1.02×10^8	−89.17 (0.08)	2.25
CaPSil4	3.22×10^9	−109.66 (0.04)	1.06×10^9	−100.64 (0.05)	1.35×10^8	−89.15 (0.02)	3.04

phosphate. This behavior was checked in the pH stability, where calcium phosphate showed a low chemical stability when exposed to acidic medium (pH < 4.0) while for nanocomposites, an improvement occurred in the chemical stability for the same pH. For example, in pH $= 1.0$, CaPSil2, CaPSil3, and CaPSil4 lixiviated 10% of original calcium. For monetite, the content of dissolved calcium was 27.2% (Fig. 6).

Conclusions

Calcium phosphate/silica nanocomposites were synthesized by using sol–gel process through controlled hydrolysis of TEOS using calcium and phosphate salts in aqueous solution. Silica was covalently incorporated onto calcium phosphate surface. ^{29}Si NMR data showed that the increasing of silica immobilization reduced the Q^3 species which contributes substantially for mass loss detected by TG. Silica/calcium phosphate nanocomposites were stable chemically at pH lower than 4.0 while the precursor phosphate dissolved under the same conditions.

Acknowledgements The authors thank CAPES and CNPq for their financial support.

References

1. Anderson J, Areva S, Spliethoff B, Lindén M. Sol-gel synthesis of a multifunctionally porous silica/apatite composite. Biomaterials. 2005;26:6827–35.
2. Borum L, Wilson OC. Surface modification of hydroxypatite. Part II. Silica. Biomaterials. 2003;24:3681–8.
3. Unger RE, Sartoris A, Peters K, Motta A, Migliaresi C, Kunkel M, Bulnheim U, Rychly J, Kirkpatrick JC. Tissue-like self-assembly in cocultures of endothelial cells and osteoblasts and the formation of microcapillary-like structures on three-dimensional porous biomaterials. Biomaterials. 2007;28:3965–76.
4. Corami A, Mignardi S, Ferrini C. Copper and zinc decontamination from single -and binary- metal solutions using hydroxyapatite. J Hazard Mater. 2007;146:164–70.
5. Hu A, Li M, Chang C, Mao D. Preparation and characterization of a titanium-substituted hydroxyapatite photocatalyst. J Mol Catal A. 2007;267:79–85.
6. Mitsionis AI, Vaimakis TC. A calorimetric study of the temperature effect on calcium phosphate precipitation. J Therm Anal Calorim. 2010;99:785–9.
7. Oudadesse H, Derrien AC, Lefloch M. Infrared and nuclear magnetic resonance structural studies vs thermal treatment of geopolymers/biphasic calcium phosphates. J Therm Anal Calorim. 2005;82:323–9.
8. Pavia DL, Lampman GM, Kriz GS. Introduction to spectroscopy. 2nd ed. New York: Saunders College Publishing; 1996.